First ground-based mesospheric measurements from central Himalayas

A. Guharay[1], A. Taori[2,*], S. Bhattacharjee[1], P. Pant[1], B. Pande[3] and K. Pandey[3]

[1]Aryabhatta Research Institute of Observational Sciences, Nainital 263 129, India
[2]National Atmospheric Research Laboratory, Gadanki 517 112, India
[3]Department of Physics, DSB Campus, Kumaun University, Nainital 263 001, India

First ground-based mesospheric temperature measurements from a central Himalayan station of India, Nainital (29.4°N and 79.5°E) have been carried out during January 2007 with the help of OH and O_2 airglow monitoring during night-time. The derived temperatures exhibit large amplitudes of ~3–6 h waves together with a longer period nocturnal tide-like feature with periodicity ~8–10 h. The observed temperatures are in agreement with the SABER derived temperatures, onboard the TIMED satellite and in less resemblance with MSIS-00 model data. The Krassovsky's analysis shows the mean η values to be ~13.4 ± 2.5 and 10.05 ± 2.3; and φ values –23.8 ± 11° and –23.5 ± 11.5° for O_2 and OH data respectively, which are higher than the reported values in the literature. The deduced vertical wavelengths are found to be ~29.6 ± 11.1 km and 43 ± 21.5 km for O_2 and OH respectively, indicating the observed waves to be upward propagating.

Keywords: Airglow, Krassovsky parameter, MLTP, mesospheric dynamics.

GRAVITY waves and tides are one of the most important neutral coupling processes throughout the earth's atmosphere. Generated at lower atmosphere, waves and tides propagate through the middle atmosphere and often they reach up to the upper atmosphere. When gravity waves and tides pass through different altitudes, the neutral density and temperatures get perturbed according to their properties and consequent to this, airglow emission intensity also gets affected[1]. For the above reason since more than a decade, airglow monitoring has been utilized as a tool to investigate the gravity wave and tidal properties, and influences in middle and upper atmosphere[2–4]. Although progress has been made to understand and characterize these waves, our understanding regarding the wave induced perturbations in temperature and intensity and their interrelation at mesospheric altitudes is far from complete.

For example, several reports are available on the characterization of gravity wave and tides using Krassovsky[5] method that study the transfer function between intensity and temperature perturbations[6–8]. Some of the studies utilize image measurements to study the momentum flux[9]. Few studies utilize multiple altitude airglow emissions to study the gravity wave growth and dissipation[10] and some of the studies interestingly show the influence of mesospheric variability in the thermosphere–ionosphere system[11]. Though these reports are geographically widespread, there are no ground based measurements from/or nearby the Himalayas. Our aim in the present article is to present the first mesospheric measurements on waves from a high altitude (~2 km above mean sea level) station Nainital (29.4°N, 79.5°E) situated in the Shivalik Ranges of central Himalayas whose unique topographic feature is expected to give spectacular wave signatures.

Instrumentation

The mesosphere lower thermosphere photometer (MLTP) is designed to study the mesosphere, thermosphere and ionosphere systems behaviour simultaneously. The MLTP utilizes seven narrow bandwidth (FWHM ~ 0.4 nm) interference filters (made by ANDOR Corporation, USA) of central wavelength ~840 and 846 nm for OH (6–2), 866 and 868 nm for O_2 (0–1), 630 nm for thermospheric $O(^1D)$ emission, 557.7 nm for lower thermospheric $O(^1S)$ emission and one filter at 857 nm for measuring background emission. The filters have transmission efficiency ~40–70% at 24°C and a low temperature coefficient of ~0.012 nm/°C. It uses three $f/2$ lens systems for collimating the incoming radiation and refocussing the image to the detector with a slit to limit the full field of view to 4°. The MLTP consists of a photo multiplier tube (R943-02 supplied by Hamamatsu, Japan) as a detector which uses GaAs(Cs) photocathode that has a very wide spectral response (~160–930 nm), a low dark count (20 counts/s at –20°C) and high quantum efficiency (~14% at 633 nm). All the filters are fixed to an aluminum plate, which is rotated by a motor system to align each of the filters with the optical axis of the instrument in a sequential manner of the observational cycle, with 10 s exposure time and a time resolution of 90 s for suitable observation. The temperature of the filter plate is controlled with a precision of better than 0.25°C by a set of 16 peltier elements and a

*For correspondence. (e-mail: taori@narl.res.in)

proportional integral derivative (PID) sensor (supplied by Melcor Inc., USA). The photon counts recorded in the computer are used to derive the temperature by ratio method as described by Meriweather[12] with errors in the temperature estimates (caused by uncertainty in the spectroscopic constants and instrumental limitations) not more than 5% which gives a temperature precision at order of ~2 K in 6 min time integration.

Results and discussions

The first ever ground-based nocturnal mesospheric OH and O_2 airglow monitoring from a high altitude (~2 km above mean sea level) central Himalayan station, Nainital (29.4°N and 79.5°E) was made on 15 and 16 January 2007. The deduced temperature variation is reported in this article.
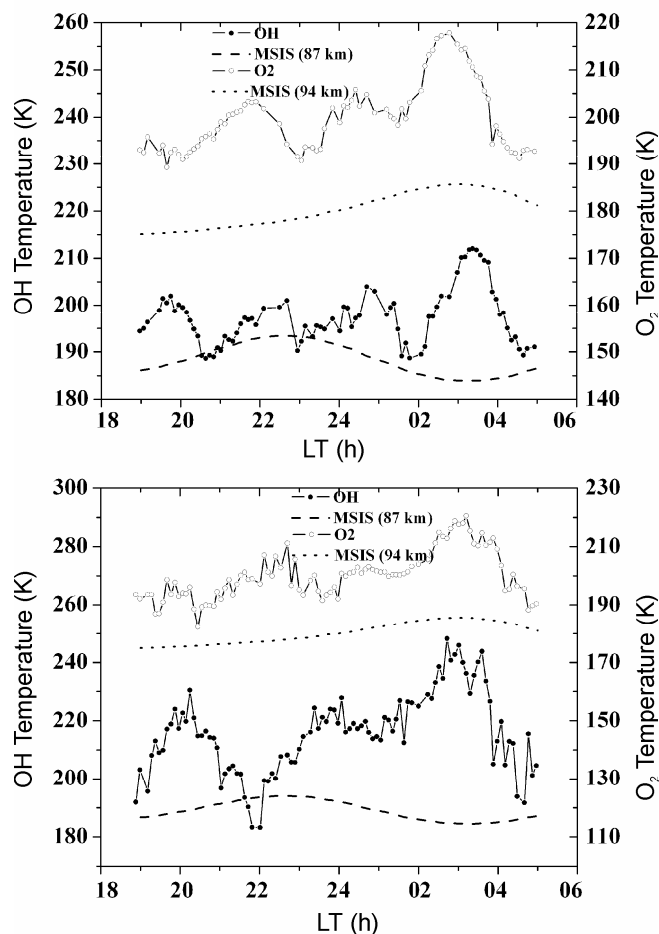
Figure 1. Nocturnal temperature variation for OH (6–2) and O_2 (0–1) data over Nainital. The upper panel shows the temperature variability for 15 January, whereas the lower panel represents the temperature for 16 January 2007. One should note the long period as well as short period features embedded on it. The symbol and solid connecting lines are the observed values, whereas dashed lines are the MSIS-00 model estimates.

Observations

Figure 1 displays the nightly variability in the mesospheric temperatures at OH and O_2 emission altitudes (centered on ~86 and 94 km respectively). The nocturnal pattern shows a long-period wave with short-period oscillatory features embedded on it. The upper panel in Figure 1 exhibits the nocturnal temperature variability of OH and O_2 data with respect to local time for 15 January 2007. It is evident that the data show the presence of multiple waves with different periodicities during 10 h of operation. Noteworthy are large ranges of temperature variability with OH temperatures varying from ~188 K to 210 K and O_2 data ranges from ~190 K to 218 K, indicating large peak to peak variability (~15% of mean temperatures). The mean values of the nocturnal temperatures are ~197 K for OH data and ~200 K for O_2 data. Together with our derived temperatures, also shown in the plot are mass spectrometer incoherent scatter (MSIS-00) (ref. 13) model estimates for 86 and 94 km altitudes. The differences in the mean values of derived OH and O_2 temperatures with the model estimated values ($T_{Observed} - T_{MSIS}$) are found to be ~11 and 20 K respectively. Such inconsistency in comparison of MSIS-00 model with our observations at different altitudes may be due to the limitations of the MSIS-00, as it is constructed from incoherent scatter measurements from the ground sites at Arecibo, Jicamarca, Millstone Hill, Malvern and St. Santin, which are mostly situated in western hemisphere. Also, it should be mentioned that the Himalayan region is unique for its peculiar topography, which may be a cause for observed mismatch. However, it is interesting to note that altitudinal temperature difference between MSIS mean temperatures ($MSIS_{86\,km} - MSIS_{94\,km} \sim 8$ K) and observed mean temperatures ($T_{OH} - T_{O_2} \sim 3$ K) compares well within the standard deviation (<10 K) on the individual night of operation.

The bottom panel in Figure 1 shows the observed temperature variability for OH and O_2 data on 16 January 2007. The temperature values were higher compared to the 15 January values (mean values ~215 K for OH and ~201 K for O_2). The ranges in the temperature variability were 190–235 K for OH and 190–220 K for O_2 data. Interestingly, the difference between the mean of observed and MSIS-00 temperature ($T_{Observed} - T_{MSIS}$) is ~25 K for OH and ~20 K for O_2 data. However, the altitudinal temperature differences between MSIS mean temperatures ($MSIS_{86\,km} - MSIS_{94\,km} \sim 10$ K) and observed mean temperatures ($T_{OH} - T_{O_2} \sim 14$ K) are somewhat in agreement. Our observed temperatures are generally higher for both the days for OH and O_2 in comparison with the MSIS-00 values, which was also noted by Chu et al.[14], using ground based Na lidar observation between 85 and 100 km from two places, Maui (20.7°N) and Starfire Optical region (35°N). They found the maximum temperature differences between lidar and MSIS-00 of the order of ~20 K.

Coincident satellite data

In coincidence with the above airglow observations, sounding of the atmosphere using Broadband Emission Radiometry (SABER) onboard the Thermosphere Ionosphere Mesosphere Energetics and Dynamics (TIMED) satellite pass was available for the midnight of 15 January operation. We have used SABER version 1.07 temperature data for comparison with our data. The SABER data has good temperature accuracy with error in the order of ±1.4 K in lower stratosphere, ±1 K in middle stratosphere and ±2 K in upper stratosphere and lower mesosphere[15]. Figure 2 plots the vertical profile of temperature obtained from SABER instrument over the latitude and longitude range 29–30°N and 79–81°E during the night observations of 15 January 2007 for a comparison. The SABER data also reveals large oscillations on 15 January 2007 similar to the MLTP observed features. SABER data shows a weighted mean (calculated over 10 km altitude range (±5 km) centered on the peak of emission altitudes as it is well known that airglow layer heights change with time round the season) temperature ~188 K at 94 km and ~206 K at 87 km during its overpass around 01 : 30 LT of 16 January, which matches closely with MLTP observed values of 196 K and 204 K respectively. One important reason for the mismatch between our observed temperatures and TIMED/SABER obtained data may be because of difference in the airglow emission layer altitudes which we have assumed to be ~86 km for OH and ~94 km for O_2 emissions.

## Evident wave signatures

To examine the predominant wave in the data, a half hourly average has been done to smooth out the short period (<0.5 h) waves. Figure 3 shows the observed 2-day mean profile of half hourly average temperature of OH and O_2 along with sinusoidal fit to data of 15 and 16 January 2007. Vertical bars represent the standard deviation, which is a measure of nocturnal variability within that particular time span. The best fit result reveals the presence of periods of ~9 ± 1 h for OH and ~10.3 ± 1.1 h for O_2 data. The observed difference in periodicity of the propagating wave may be due to the wave–mean wind interaction between these two altitudes. The derived wave amplitudes are ~8.2 ± 3.2 K for OH and ~6.9 ± 2.6 K for O_2 temperature data. It is evident from the plot that OH is having higher variability compared to O_2, might be because of higher wave activity persisting during the observation period in that region. Of importance here is the presence of tide-like (possibly an interference of semidiurnal tide within the 10 h observation window) feature in the data with wave period of ~8–10 h with the phase at ~02.10 h and 02.27 h for O_2 and OH, respectively. The global scale wave model (GSWM-02)[16]

results for 30°N, 80°E exhibited the semi-diurnal tides to be of amplitudes ~6.59 K and 4.92 K and phases at ~02.80 and 03.07 LT h for 94.6 km and 86.3 km, respectively
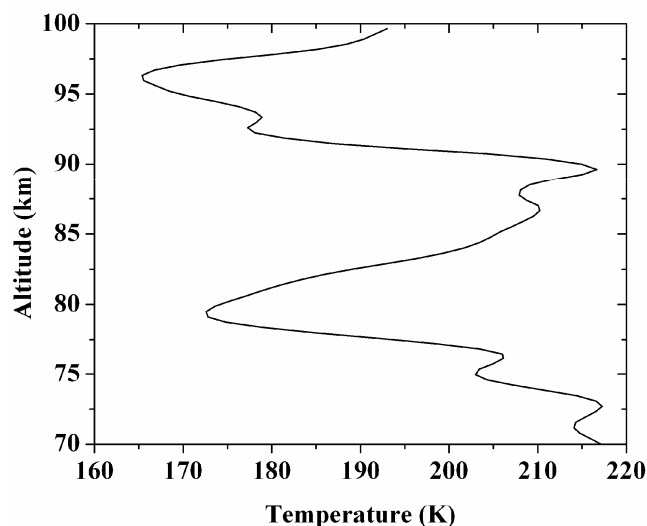
Figure 2. Vertical profile of TIMED/SABER temperature profile for the comparison with the midnight observations of 15 January 2007 during its pass over 29–30°N and 79–81°E grid centred over Nainital.
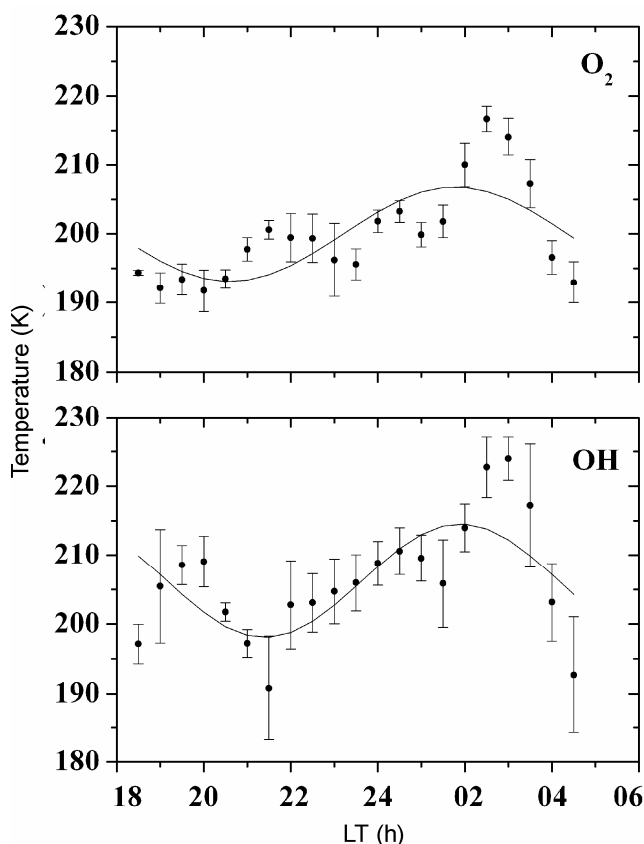
Figure 3. Average temporal profile of OH and O_2 temperature with a long period best-fit sinusoidal model. The vertical bars represent the standard deviation on hourly mean data, a measure of variability.

for January which matches closely for our observed values. Our observation which reveals decreasing amplitude of the principal wave with altitude unlike GSWM may be because of local dissipation processes dominating over there, and is not detected by the model, although the amplitude uncertainties restrict us to conclude anything unwaveringly. Though semidiurnal amplitudes from GSWM-02 estimates are somewhat different from the observed values, our data limited only for two nights with 10 h observation span are not sufficient for a suitable comparison hence, this aspect is not perused further in this article.

For characterization of the nocturnal wave features in the data, we carried out wavelet analysis which is an improved version of Fourier transform and provides a time-frequency spectrum of wave activity useful for non-stationary time domain signal using multi-resolution analysis[17]. We have used Morelet wavelet as a mother wavelet, which is actually a plane wave modulated by a Gaussian function. Cross wavelet spectrum has also been derived from OH and O_2 spectra, which reveals the common wave packets co-existing in both the spectra, in other words we can say that it extracts the propagating/similar wave components and subdues the small scale non-progressive (probably dissipated somewhere in between two airglow layers) oscillations from the individual wavelet spectra. We have plotted the magnitude of wavelet co-efficient as a function of time and period in Figure 4, which is derived by taking integration of the product of signal and mother wavelet over all the time and scale (1/frequency) span. The upper, middle and lower panels represent the wavelet spectrum for O_2, OH and a cross wavelet spectrum respectively. The plot reveals that a number of wave packets of various periodicities exist over different time span in the OH and O_2 temperature data. The O_2 spectrum reveals the dominance of 5–6 h wave with their peak amplitudes around 19, 21–22, 23–01, 02–03 LT h. Also, a less dominant long period ~8–9 h wave is existing around 21–23 and 01–03 LT h. At the same time, the OH spectrum also contains small period waves (3–4 h) scattered throughout the observation span, whereas the long period (~8–9 h) waves are present around 18.5, 21–23, 01–03 LT h. However, the cross wavelet spectrum shows 8–9 h waves to be the dominant one around 21–23 and 01–03 LT h. Also 3–4 h waves are present with less magnitude around 03 and 05 LT h. It is important to note that the cross wavelet spectrum agrees well with the wave characteristics as already revealed in the best fit analysis.

Long period wave characteristics

As noted above, the simultaneous temperature variability in OH and O_2 data reveals large amplitudes of short period as well as tide-like oscillations with periodicity ~8–10 h

wave. For characterization of the observed long period wave, we estimate Krassovsky's η values[5], which is defined as $\eta = |\eta| e^{i\varphi}$, where

$$|\eta| = \frac{(\Delta I / \langle I \rangle)}{(\Delta T / \langle T \rangle)}. \tag{1}$$

The ΔI and ΔT are perturbation amplitudes (caused by the propagating wave) in band intensity and temperature respectively, $\langle I \rangle$ and $\langle T \rangle$ are the mean band intensity and temperature. The phase part Φ can be defined as,

$$\Phi = \Phi_I - \Phi_T, \tag{2}$$

where Φ_I and Φ_T are the phase values of the wave in band intensity and temperature respectively. Together with the above, vertical wavelength can also be calculated with the help of the following equation[18]

$$\lambda_z = \frac{2\pi \gamma H}{(\gamma - 1)|\eta| \sin(\varphi)}, \tag{3}$$

where $\gamma = C_p / C_v = 1.4$ assuming that the atmosphere is diatomic molecule dominated. Scale height (H) can be taken as 6 km at this altitude.

As explained by Guharay et al.[19] with the best-fit method in temperature and band intensities, the amplitude
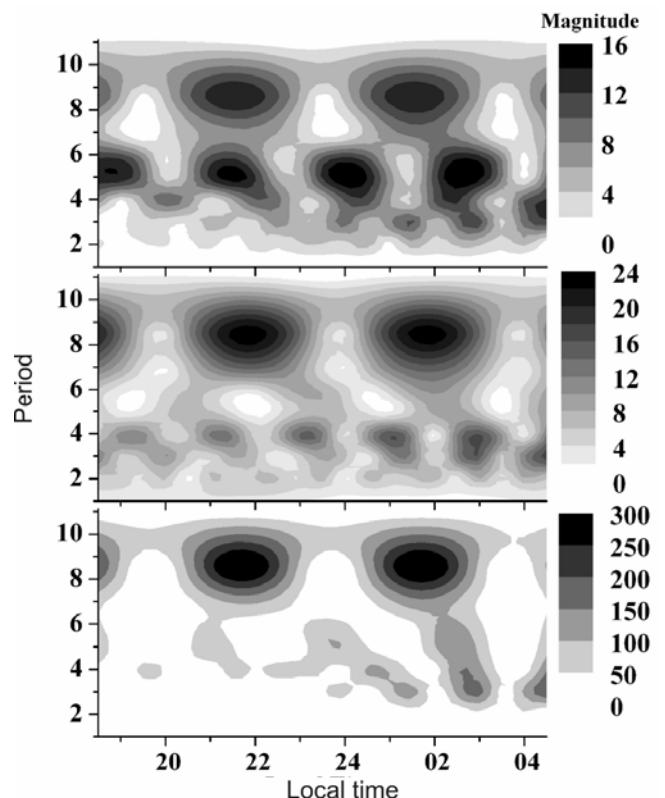
Figure 4. Continuous wavelet spectra of the nocturnal temperature data. Upper, middle and lower panels exhibit wavelet spectrum for O_2, OH and their cross wavelet spectrum respectively.

Table 1. Deduced wave characteristics including Krassovsky parameters and vertical wavelength for the present study for O_2 and OH data together with the values reported by other investigators

Time	Emission layer	Period (h)	$|\eta|$	Φ (degree)	λ_z (km)	Reference
15 January 2007	O_2	9.42 ± 1.1	14.3 ± 2.7	−13.2 ± 5.9	−40.5 ± 19	Present study
	OH	9.75 ± 1.4	15.5 ± 4.4	−18.3 ± 13.2	−26.9 ± 20	
16 January 2007	O_2	11.83 ± 1.2	12.4 ± 2.2	−34.4 ± 21.5	−18.8 ± 10	
	OH	11.76 ± 1.7	4.6 ± 1.0	−28.7 ± 18.8	−59 ± 38	
October–December 1996, 1997	OH	~8	6 ± 2	−51 ± 21		3
July 2002	O_2	~8	7.04 ± 0.65	−29.8 ± 1.7	−49 ± 5.7	19
	OH	~8	3.27 ± 0.44	−33.6 ± 2	−80.8 ± 15.4	
1986, 1987, 1992, 1996	O_2	12.6 ± 0.7	7.2 ± 0.5	−36	−36.4 ± 3.1	7
	OH		5.5 ± 0.6	−66	−27.7 ± 2.8	
1998–2003	O_2	~12	5.89	−32.3	−40.6	20
	OH		18.1	−66.3	−9.97	
January 1991	OH	~8	2.5 ± 0.5	−30 ± 15		23
21 December 1993	OH	~8–9	8.8 ± 1.7	−107 ± 9	−28 ± 11	22
31 December 1993	OH	~8–9	2.8 ± 0.7	−12 ± 20	−79 ± 18	
1983–1992	O_2	~8	7.1			2
	OH		4.9			
December 1984	OH	12	3.2 ± 0.9	6 ± 16		21
		3.7	4.3 ± 1.3	−12 ± 12		

of Krassovsky parameter for principal wave (~10 h periodicity) was found to be 14.3 ± 2.7 and 15.5 ± 4.4 on 15 January and 12.4 ± 2.2 and 4.6 ± 1.0 on 16 January for O_2 and OH respectively. When compared with the values obtained elsewhere, we find that our observed η values (except η_{OH} on 16 January) from a low latitude station, Nainital in central Himalayas on both the days show higher values (>10) compared to most of the results obtained from low-latitudes[2,19], mid-latitudes[3,7,20] and high-latitudes[21–23]. The detailed comparison of the same is shown in Table 1. In this context, it is important to note that higher values of η in OH airglow emission for terdiurnal waves were also found by Oznovich et al.[24] and Garcia and Solomon[25]. Of equal importance here is the fact that the value of Krassovsky's parameter is strongly dependent on wave-induced fluctuation of airglow emission layer density and chemical reactions taking place at those altitudes. The eddy kinematic viscosity and eddy thermal diffusivity are important factors for modifying the η (ref. 24), which can be significantly different from place to place and specific to the geographical locations. However, our derived phase values are consistent with those reported earlier. Our observed vertical wavelengths (<60 km) show significant differences from one night to the other night, with clear case of propagating wave and no possible evanescence. It appears that though the propagation characteristics of waves over Nainital are similar to other locations, transfer function from density perturbations to the temperatures are somewhat lower than other places. This can only be tested in future through rigorous observations.

1. Hines, C. O. and Tarasick, D. W., Layer truncation and the Eulerian/Lagrangian duality in the theory of airglow fluctuations induced by gravity waves. *J. Atmos. Sol. Terr. Phys.*, 1997, **59**, 327–334.
2. Takahashi, H., Sahai, Y., Batista, P. P. and Clemesha, B. R., Atmospheric gravity wave effect on the airglow O_2 (0–1) and OH (9–4) band intensity and temperature variations observed from a low latitude station. *Adv. Space Res.*, 1992, **12**, 131–134.
3. Taylor, M. J., Gardner, L. C. and Pendleton Jr, W. R., Long-period wave signatures in mesospheric OH Meinel (6,2) band intensity and rotational temperature at mid-latitudes. *Adv. Space Res.*, 2001, **27**, 1171–1179.
4. Taori, A., Taylor, M. J. and Franke, S., Terdiurnal wave signatures in the upper mesospheric temperature and their association with the wind fields at low latitudes (20°N). *J. Geophys. Res.*, 2005, **110**, in press.
5. Krassovsky, V. I., Infrasonic variations of OH emission in the upper atmosphere. *Annu. Geophys.*, 1972, **28**, 739–746.
6. Viereck, R. A. and Deehr, C. S., On the interaction between gravity waves and the OH Meinel (6–2) and O_2 atmospheric (0–1) bands in the polar night airglow. *J. Geophys. Res.*, 1989, **94**, 5397–5404.
7. Reisin, E. R. and Scheer, J., Characteristics of atmospheric waves in the tidal period range derived from zenith observations of O_2 (0–1) atmospheric and OH (6–2) airglow at lower midlatitudes. *J. Geophys. Res.*, 1996, **101**, 21223–21232.
8. Taori, A. and Taylor, M., Characteristics of wave induced oscillations in mesospheric O_2 emission intensity and temperatures. *Geophys. Res. Lett.*, 2006, **33**, L01813.
9. Swenson, G. R. and Mende, S. B., OH emissions and gravity waves (including a breaking wave) in all-sky imagery from Bear Lake, Utah. *Geophys. Res. Lett.*, 1994, **21**, 2239–2242.
10. Taori, A., Guharay A. and Taylor, M. J., On the use of simultaneous measurements of OH and O_2 emissions to investigate wave growth and dissipation. *Ann. Geophys.*, 2007, **25**, 639–643.
11. Vineeth, C. et al., Investigation of the response of equatorial MLTI region during a partial solar eclipse through ground-based daytime optical technique. *J. Geophys. Res.*, 2008, **113**, A03302.

12. Meriwether Jr, J. W., Ground based measurements of mesospheric temperatures by optical means. *MAP Handbook*, 1984, **13**, 1–18.

13. Picone, J. M., Hedin, A. E., Drob, D. P. and Aikin, A. C., NRLMSISE-00 empirical model of the atmosphere: Statistical comparisons and scientific issues. *J. Geophys. Res.*, 2002, **107**, 1468.

14. Chu, X., Gardner, C. S. and Franke, S. J., Nocturnal thermal structure of the mesosphere and lower thermosphere region at Maui, Hawaii (20.7°N), and Starfire Optical Range, New Mexico (35°N). *J. Geophys. Res.*, 2005, **110**, D09S03.

15. Remsberg, E. E. *et al.*, Assessment of the quality of the Version 1.07 temperature-versus-pressure profiles of the middle atmosphere from TIMED/SABER. *J. Geophys. Res.*, 2008, **113**, D17101.

16. Hagan, M. E. and Forbes, J. M., Migrating and nonmigrating diurnal tides in the middle and upper atmosphere excited by tropospheric latent heat release. *J. Geophys. Res.*, 2002, **107**, 4754.

17. Torrence, C. and Compo, G., A practical guide to wavelet analysis. *Bull. Am. Meteorol. Soc.*, 1998, **79**, 61–78.

18. Tarasick, D. W. and Hines, C. O., The observable effects of gravity waves in airglow emission. *Planet. Space Sci.*, 1990, **38**, 1105–1119.

19. Guharay, A., Taori, A. and Taylor, M., Summer-time nocturnal wave characteristics in mesospheric OH and O_2 airglow emissions. *Earth Planet. Space*, 2008, **60**, 973–979.

20. Lopez-Gonzalez, M. J. *et al.*, Tidal variations of O_2 atmospheric and OH(6–2) airglow and temperature at mid-latitude from SATI observations. *Ann. Geophys.*, 2005, **23**, 3579–3590.

21. Sivjee, G. G., Walterscheid, R. L., Hecht, J. H., Hamwey, R. M., Schubert, G. and Christensen, A. B., Effects of atmospheric disturbances on polar mesopause airglow OH emissions. *J. Geophys. Res.*, 1987, **92**, 7651–7656.

22. Oznovich, I., McEwen, D. J. and Sivjee, G. G., Temperature and airglow brightness oscillations in the polar mesosphere and lower thermosphere. *Planet. Space Sci.*, 1995, **43**, 1121–1130.

23. Drob, D. P., Ground-based optical detection of atmospheric waves in the upper mesosphere and lower thermosphere, Ph D thesis, University of Michigan, 1996.

24. Oznovich, I., Walterscheid, R. L., Sivjee, G. G. and McEwen, D. J., On Krassovsky's ratio for ter-diurnal hydroxyl oscillations in the winter polar mesopause. *Planet. Space Sci.*, 1997, **45**, 385–394.

25. Garcia, R. R. and Solomon, S., The effect of breaking gravity waves on the dynamics and chemical composition of the mesosphere and lower thermosphere. *J. Geophys. Res.*, 1985, **90**, 3850–3868.